DIESEL COMBUSTION AND EMISSIONS FORMATION USING MULTIPLE 2-D IMAGING DIAGNOSTICS

J.E. Dec
Sandia National Laboratories

INTRODUCTION

Understanding how emissions are formed during diesel combustion is central to developing new engines that can comply with increasingly stringent emission standards while maintaining or improving performance levels. Laser-based planar imaging diag-nostics are uniquely capable of providing the temporally and spatially resolved information required for this understanding.

Using an optically accessible research engine, a variety of two-dimensional (2-D) imaging diagnostics have been applied to investigations of direct-injection (DI) diesel combustion and emissions formation. These optical measurements have included the following laser-sheet imaging data: Mie scattering to determine liquid-phase fuel distributions, Rayleigh scattering for quantitative vapor-phase-fuel/air mixture images, laser induced incandescence (LII) for relative soot concentrations, simultaneous LII and Rayleigh scattering for relative soot particle-size distributions, planar laser-induced fluorescence (PLIF) to obtain early PAH (poly-aromatic hydrocarbon) distributions, PLIF images of the OH radical that show the diffusion flame structure, and PLIF images of the NO radical showing the onset of NO_x production. In addition, natural-emission chemiluminescence images were obtained to investigate autoignition.

These imaging diagnostics have been used to map out the processes occurring in the cylinder of an operating diesel engine from the start of injection, through autoignition, the premixed burn, and the first part of the mixing-controlled burn (*i.e.* until the end of injection). Each diagnostic provides important information on the corresponding aspect of diesel combustion; however, combining the results of the individual measurements provides an even greater understanding of the combustion and emissions formation processes. This more complete understanding leads to a description or "conceptual model" of diesel combustion [1].

In the following sections the experimental setup is described, and the image data showing the most relevant results are presented. Then the conceptual model of diesel combustion is summarized in a series of idealized schematics depicting the temporal and spatial evolution of a reacting diesel fuel jet during the time period investigated. Finally, recent PLIF images of the NO distribution are presented and shown to support the timing and location of NO formation hypothesized from the conceptual model.

EXPERIMENT DESCRIPTION

A schematic of the optically accessible engine used for the imaging measurements is shown in Fig.1. The engine is a single-cylinder, direct-injection, 4-stroke diesel engine based on a Cummins N-series production engine. The N-series engine is typical of heavy-duty size-class diesel engines, with a bore of 140 mm and a stroke of 152 mm. These dimensions are retained in the optical-access engine, and a production Cummins N-series cylinder head is used so that the production engine intake port geometry is also preserved.

The design of this engine utilizes a classic extended piston with piston-crown window. Additional windows located around the top of the cylinder wall provide the orthogonal optical access required for the two-dimensional (planar) laser imaging diagnostics. These

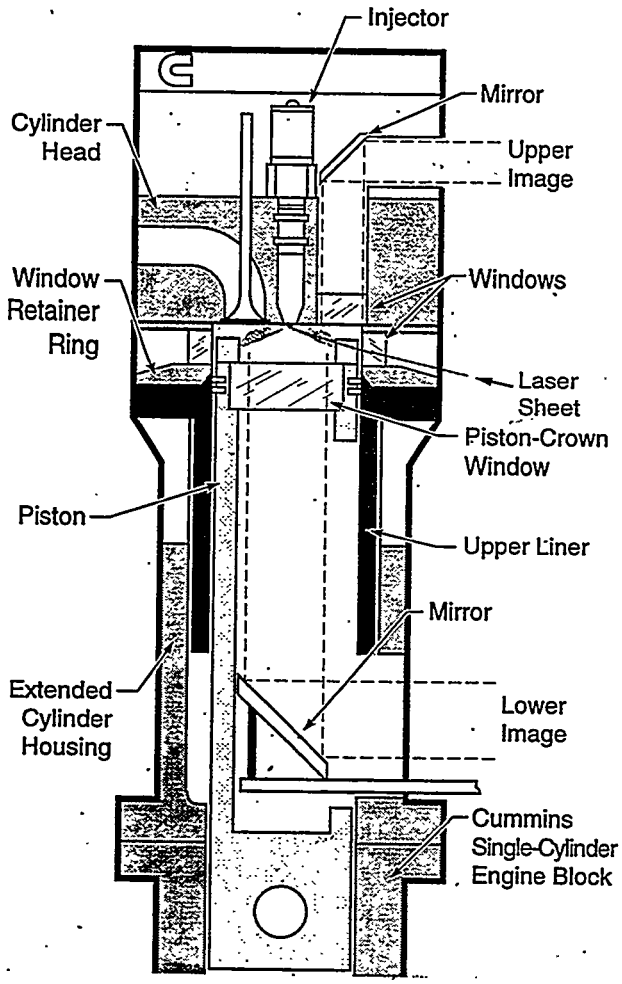

Figure 1. Schematic of the optical-access diesel engine showing the laser sheet along the fuel jet axis. Images were obtained through both the cylinder-head window (upper image) and the piston-crown window (lower image).

windows allow the laser sheet to enter the cylinder along the axis of the fuel jet (see Fig. 1) or horizontally. A window in the cylinder head replaces one of the two exhaust valves to obtain a view of the squish region and the outer portion of the combustion bowl. A complete description of the engine may be found in Ref. [2].

The experiments were conducted at a medium speed (1200 rpm) operating condition with a motored TDC (top dead center) temperature and pressure of 992° K and 5.0 MPa, which are representative diesel-engine conditions. Before conducting the experiments the engine was heated to 368° K (95°C) by means of electrical heaters on the "cooling" water and lubricating oil circulation systems. To minimize the rate of window fouling and to avoid overheating, the engine was fired once every 10th or 20th engine cycle, at which time the data were acquired. A complete discussion of the operating conditions and fuels used for the experiments may be found in Ref. [1].

Figure 2 presents a typical plot of the cylinder pressure, injector needle lift, and apparent heat release rate. As is typically found in diesel combustion, the apparent heat release rate curve in Fig. 2 first goes negative just after the start of injection as fuel vaporization cools the in-cylinder air. Then, after a few degrees, the combustion energy release exceeds that required for vaporizing the fuel, and the apparent heat release rises rapidly. The heat release rate curve then goes up through a local maximum and drops back down before rising again more slowly through a second local maximum. The initial sharp rise and fall is due to the rapid combustion of fuel that has premixed with air during the ignition delay period, and it is commonly referred to as the "premixed burn" or the "premixed burn spike". The second, broader hump in the curve is due to the mixing-controlled combustion and is commonly referred to as the "mixing-controlled burn".

Several different lasers, laser-sheet configurations, and camera setups were used for the various imaging data presented in this article. The laser sheets were typically about 25 mm wide and 250 to 300 mm thick at the probe volume. As shown in Fig.3, the laser sheet entered the combustion chamber through one of the windows at the top of the cylinder wall which was in line with one of the fuel jets. The laser sheets were oriented either horizontally or along the fuel jet axis, and images were acquired through both the piston-crown and cylinder-head windows with either one or two gated, intensified CCD video cameras. Various lens and filter combinations were used as appropriate. For some experiments, the piston bowl rim was cut out in line with

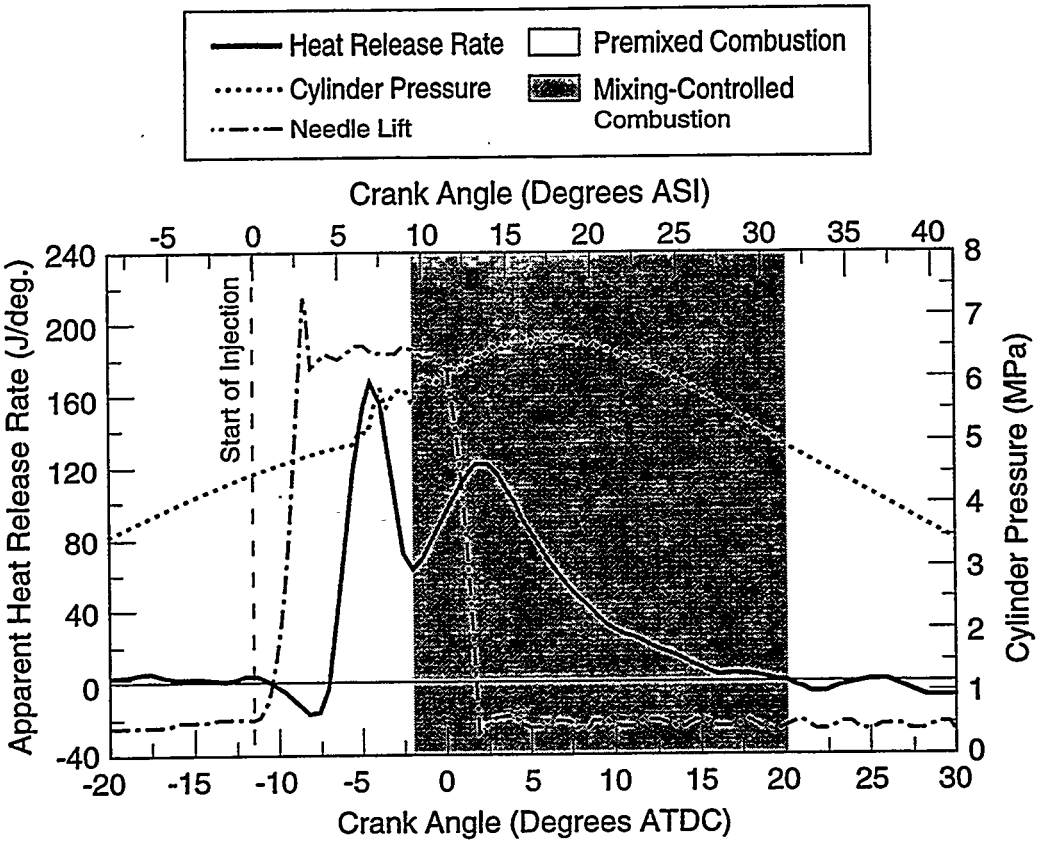

Figure 2. Apparent heat release rate, cylinder pressure, and injector needle lift for the low fuel loading (ϕ=0.25) at the base operating condition (TDC temperature = 992 K, TDC density = 16.6 kg/m^3). The engine speed is 1200 rpm, and the data are ensemble-averaged over 20 cycles.

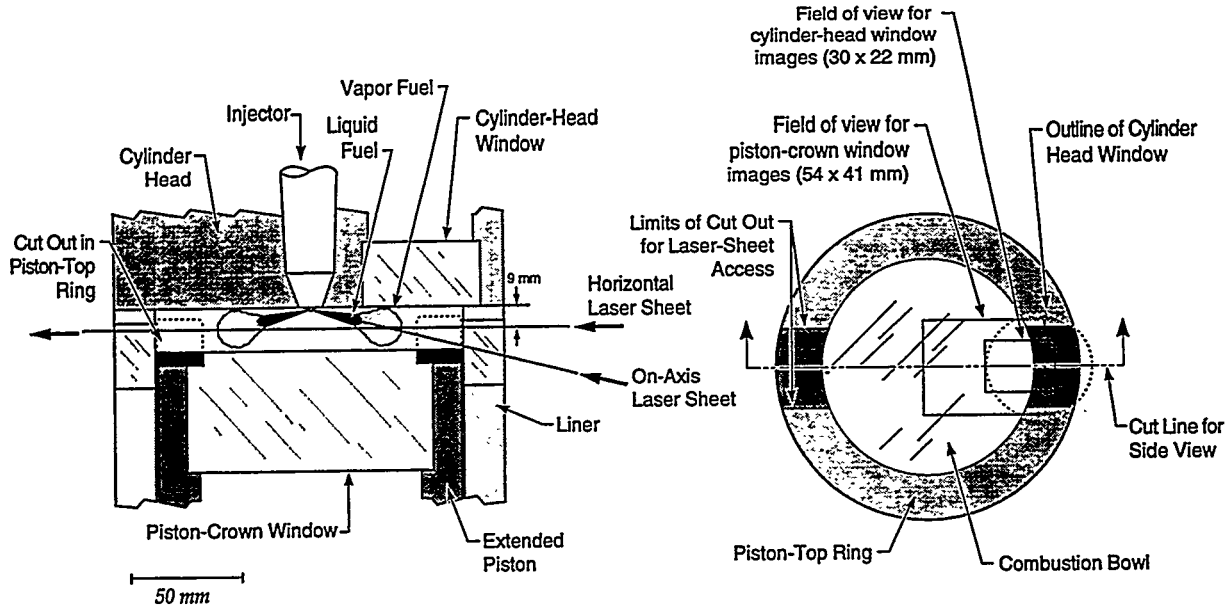

Figure 3. Geometry and optical configuration of the combustion chamber with cut outs in the rim for laser access. The schematic at the left shows a side view of the combustion chamber and the two laser-sheet orientations. At the right is a top view of the piston and typical fields of view for images obtained through both piston-crown and the cylinder-head windows. The piston is shown at the TDC position.

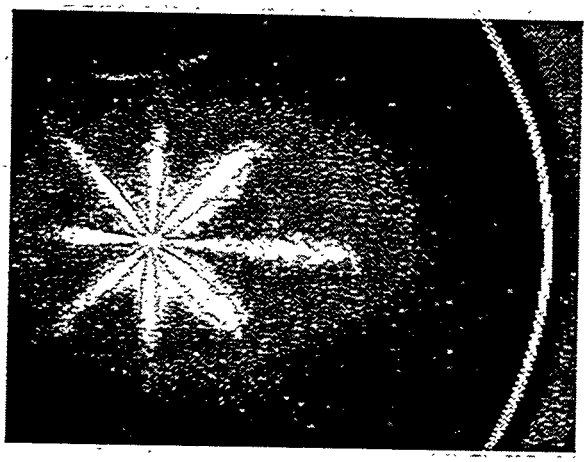

Figure 4. Liquid-phase fuel images show that all the fuel vaporizes within a characteristic length (~25 mm for the base operating condition) from the injector. See Ref. [3].

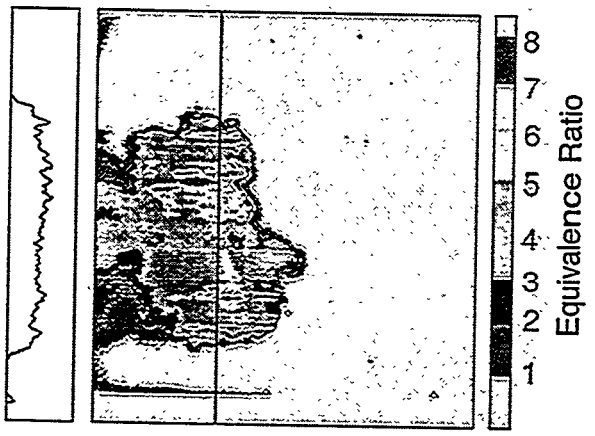

Figure 5. Quantitative vapor fuel images show that downstream of the maximum liquid penetration, the fuel and air are mixed to and equivalence ratio of 2 to 4. This relatively uniform mixture is separated from the surrounding air by a sharp transition as shown in the plot at the left. See Ref. [4].

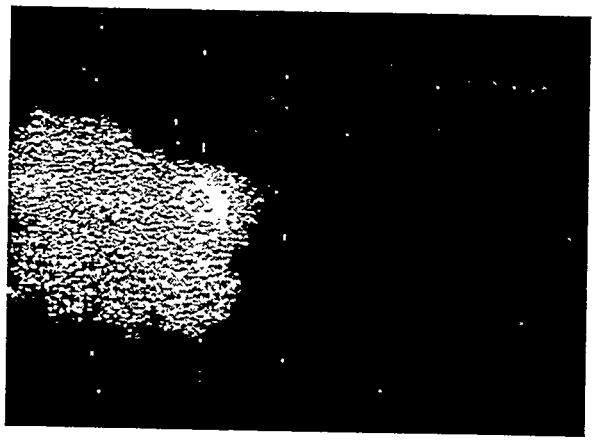

Figure 6. Chemiluminescence imaging shows auto-ignition occurring across the downstream portion of the fuel jet. See Ref. [5].

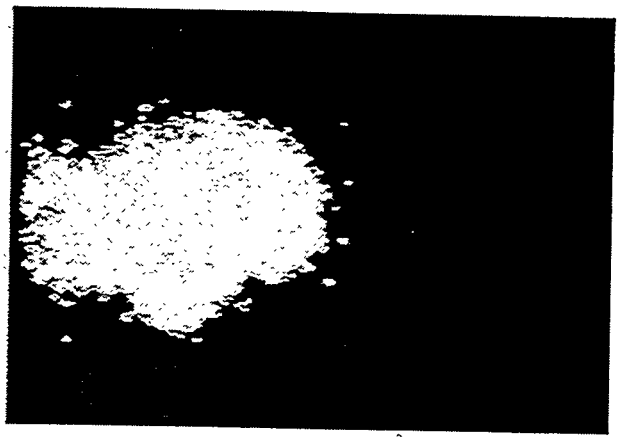

Figure 7. PAHs form throughout the cross-section of the downstream portion of the fuel jet immediately following fuel breakdown at the start of apparent heat release. See Ref. [1].

Figure 8. LII soot images show that soot forms throughout the cross-section of the fuel jet beginning just downstream of the liquid-fuel region. See Refs. [1,5].

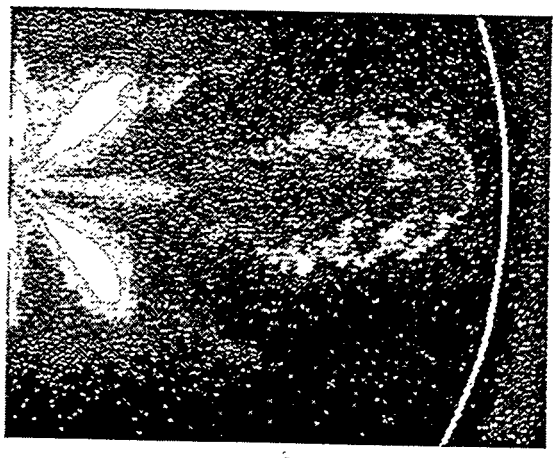

Figure 9. OH radical images show that the diffusion flame forms at the jet periphery subsequent to an initial fuel-rich premixed combustion period. See Ref. [6].

the laser sheet to permit the laser sheet to enter the combustion chamber near TDC. The intake-air temperature and pressure were adjusted to maintain the same TDC conditions despite the reduction in compression ratio resulting from the cutouts.

LASER SHEET IMAGING DATA

As mentioned above, the conceptual model of diesel combustion presented in the next section has been derived by combining the results from a variety of 2-D imaging diagnostics. Because the imaging data have been described in detail elsewhere, only a summary will be presented here. Figures 4 - 9 show typical images of most of the data types along with a brief descriptions of the most significant findings. Additional information may be found in the references given the figure captions.

Although Figs. 4 - 9 show images at only a single instant during the combustion event, temporal sequences of images were actually acquired with each of the diagnostics. An example of this is given in Fig. 10. This figure shows a temporal sequence of soot images from 7° to 17° after the start of injection (ASI) for three different imaging diagnostics, as noted at the left. These images show how the soot volume fraction and particle-size distribution develop within the reacting fuel jet in a diesel engine [1,7].

CONCEPTUAL MODEL OF DI DIESEL COMBUSTION

This section presents a series of schematics that combine the information from the individual imaging measurements into a comprehensive picture of DI diesel combustion.

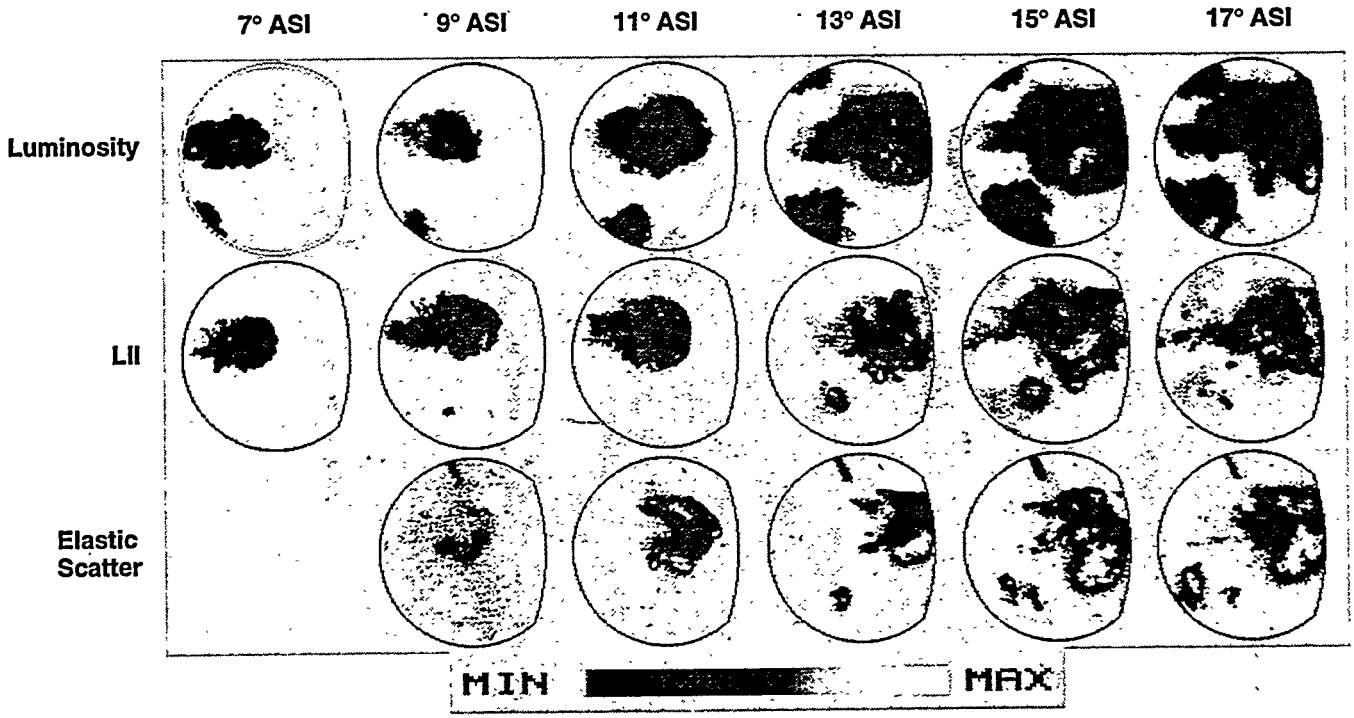

Figure 10. A temporal sequence of natural soot luminosity, laser-induced incandescence (LII), and elastic-scatter images. The crank angle degree ASI is given at the top of each set. The average equivalence ratio is 0.43, and the engine speed is 1200 rpm.

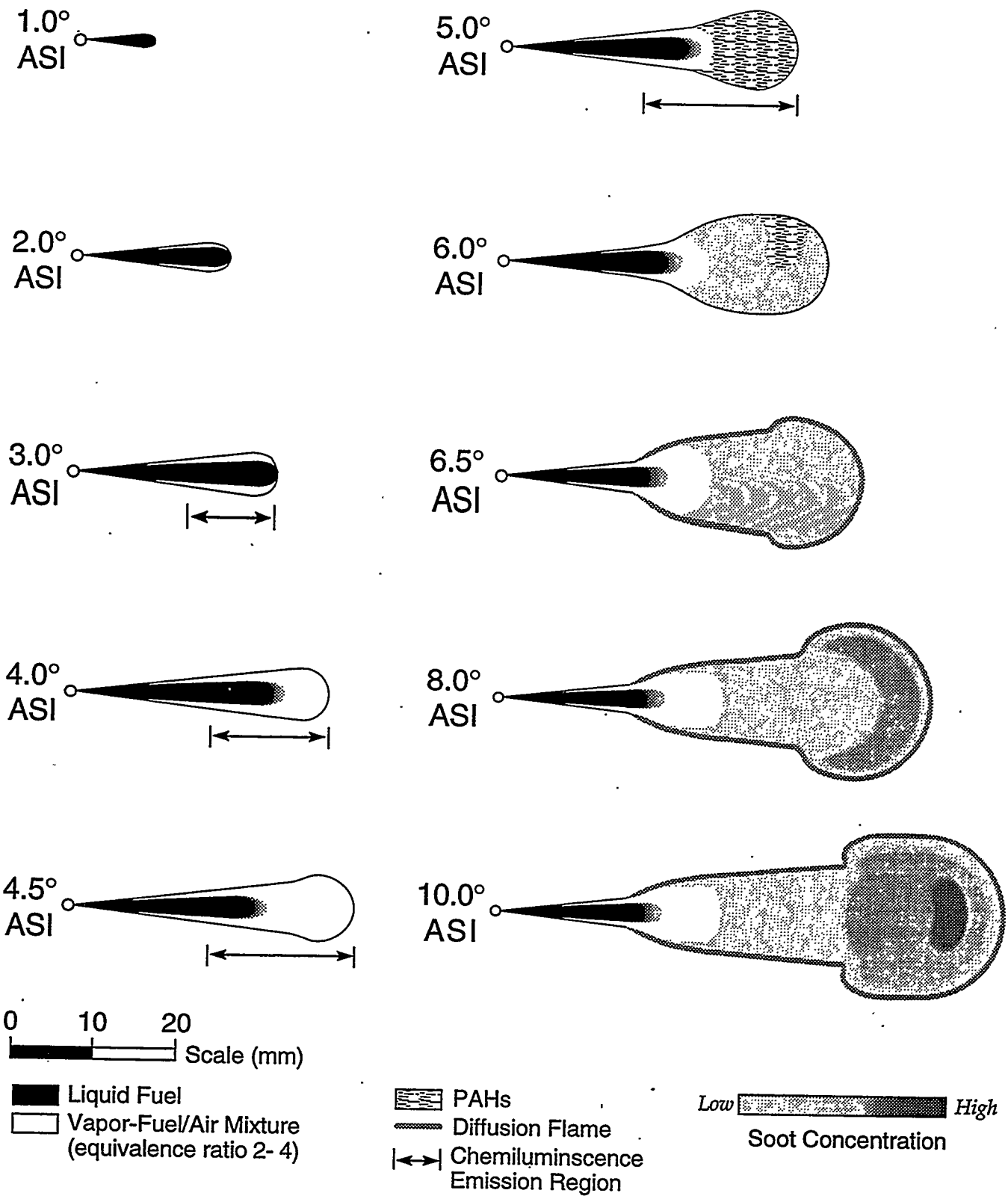

Figure 11. A temporal sequence of schematics showing how DI diesel combustion evolves from the start of injection up through the early part of the mixing-controlled burn. The temporal and spatial scales depict combustion for the base operating condition (a typical diesel engine condition) with an injection duration extending beyond the sequence shown. The crank angle degree ASI (after the start of injection) is given at the side of each schematic (1° = 139 μs).

These composite schematics represent idealized cross-sectional slices through the midplane of the jet, and they show conceptually how DI diesel combustion occurs in the absence of wall interactions and swirl. These schematic images depict the typical operating condition described above. For production engines the amount of turbocharger boost, intercooling, and injector characteristics can vary greatly, affecting both the temporal and spatial scaling (see for example Refs. [3, 8]).

Figure 11 gives a temporal sequence of schematics showing the development of a diesel fuel jet from the start of injection, through the premixed burn, and into the first part of the mixing-controlled burn. Initially, liquid fuel penetrates across the chamber, entrains hot in-cylinder air, and begins to vaporize. By 3.0° ASI, the tip of the fuel jet has penetrated about 25 mm from the injector, and sufficient air entrainment has occurred so that all the fuel is vaporized beyond this characteristic length (Fig. 4). The vapor-fuel/air mixture then penetrates on across the chamber, and a head vortex eventually develops as is typical of penetrating gas-phase jets. By 4.5° ASI, the leading portion of the jet contains a "relatively uniform" fuel/air mixture with equivalence ratios ranging from about 2 to 4 (Fig. 5).

The exact point of autoignition is not well defined either temporally or spatially. Some weak chemiluminescence occurs over the downstream portion of all the jets as early as 3.5° ASI. (This is indicated by the black arrows in Fig. 11.) As the jet penetrates, the chemiluminescence region grows and the signal becomes brighter. By 4.5° ASI, which coincides with the start of the rapid rise in the apparent heat release rate (see Fig. 2), most of the chemiluminescence is coming from the large region of vapor-fuel/air mixture in the leading portion of the jet (Fig. 6). Then, within 70 μs (5.0° ASI) the planar images show that the fuel breaks down across the cross section of the vapor-fuel/air mixture at the front of the jet, and PAHs (poly-aromatic hydrocarbons) form throughout this region (Fig. 7). These planar imaging measurement

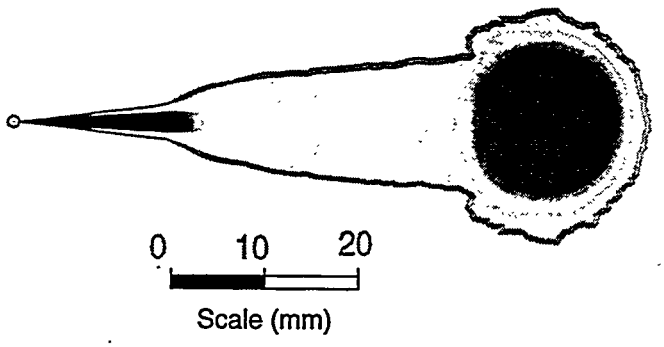

Figure 12. A schematic showing the conceptual model of DI diesel combustion derived from laser-sheet imaging for a typical time during the first part of the mixing controlled burn (*i.e.* prior to the end of injection). The color coding is the same as that given in Fig. 11.

indicate that the majority of the premixed burn occurs volumetrically in the fuel-rich (equivalence ratio 2 - 4) mixture in the leading portion of the jet.

At 6.0° ASI, small soot particles appear throughout large portions of the cross-section of the downstream region of the fuel jet at locations that vary from cycle to cycle. These small soot particles are arising from the fuel-rich premixed burn. By 6.5° ASI, soot is found throughout the cross-section of the downstream region of the jet.

Also at 6.5° ASI, a diffusion flame forms at the jet periphery between the products of the fuel-rich premixed burn (which contain a significant quantity of unconsumed fuel) and the surrounding air. This thin diffusion flame (see Fig. 9) completely encircles the downstream portion of the jet (as indicated in the schematic) just prior to the midpoint of the premixed burn spike in the apparent heat release rate. In addition, the soot particles become larger in a thin layer around the jet periphery (not shown in the schematic), due to some effect of the diffusion flame. However, it is important to note that there is no indication of a corresponding increase in soot concentration (volume fraction) at the jet periphery with the formation of the diffusion flame.

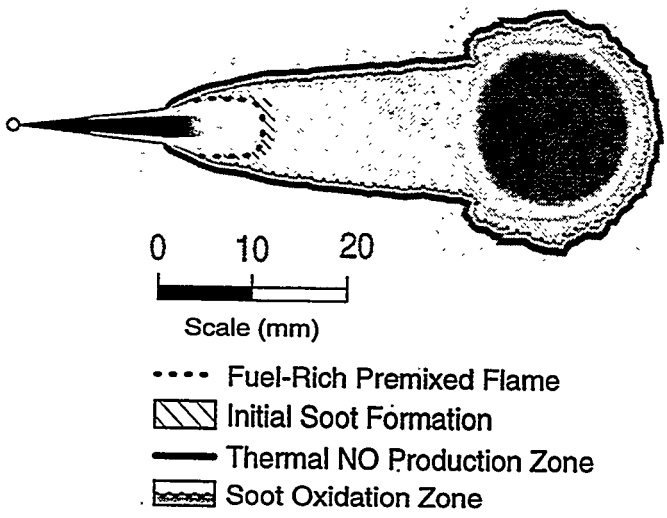

Figure 13. A schematic of the conceptual model from Fig. 12 with additional features (fuel-rich premixed flame, initial soot formation, soot oxidation, and NO formation zones) that are indicated by the data but have not yet been verified. The color coding is the same as Figs. 11 and 12 except for the additional colors given in the legend at the bottom.

Through the remainder of the premixed burn, the jet continues to grow and penetrate across the chamber, and the soot concentration continues to increase. By the end of the premixed burn (9.0° ASI) small soot particles are present throughout the jet cross section beginning approximately 27 mm from the injector. Soot particle size and concentration both increase moving down the jet with the largest soot particles and highest concentrations appearing in the head vortex.

As the combustion transitions to being purely mixing-controlled, the overall appearance of the jet shows only moderate changes, as seen in the 10° ASI schematic of Fig. 11. In fact, the jet appearance remains approximately the same up through the end of fuel injection, except that it grows larger and the soot concentrations increase. Figure 12 presents a typical schematic of the conceptual model during the mixing-controlled burn, prior to the end of fuel injection. No attempt has been made to extend the model beyond the end of fuel injection, because data are insufficient. Temporally, the schematic in Fig. 12 follows the last one in the sequence in Fig. 11; however, the size is only "representative," since a real jet grows across the time period represented. In addition, the jet boundaries in Fig. 12 have been drawn with a ragged appearance to suggest the turbulent nature of a real diesel jet.

The schematics in Figs. 11 and 12 show only the features of the reacting diesel fuel jet that have been verified by experiment. Figure 13 is a reproduction of Fig. 12 to which additional expected (hypothesized) features have been added. These additional features include: 1) a fuel-rich premixed reaction zone that leads to the onset of small soot particles throughout the jet cross section at about 27 mm from the injector; 2) a soot oxidation zone at the diffusion flame; and 3) an NO formation zone on the lean side of the diffusion flame. A complete discussion of this conceptual model of DI diesel combustion and the reasons for these additional expected features may be found in Ref. 1.

NO IMAGING DATA

Subsequent to developing the conceptual model of DI diesel combustion presented in Figs. 11 - 13, PLIF images have been obtained of the NO molecule distribution in the reacting diesel fuel jet. Figure 14 presents a temporal sequence of NO PLIF images (right) along with elastic-scatter images (left) during the early stages of DI diesel combustion. The elastic-scatter images provide a reference to determine how the combustion is proceeding. The images were obtained through the cylinder-head window using a horizontal laser sheet as shown in Fig. 3. Because of the limited field of view, only the leading portion of the fuel jet can be seen at the left in the images.

In the elastic-scatter images the bright region across the center and at the right of the field of view is Rayleigh scattering from the in-cylinder air. In the first two elastic-scatter images, the tip of the fuel jet is entering the field of view at the left and is evident as a darker region because the premixed burn is

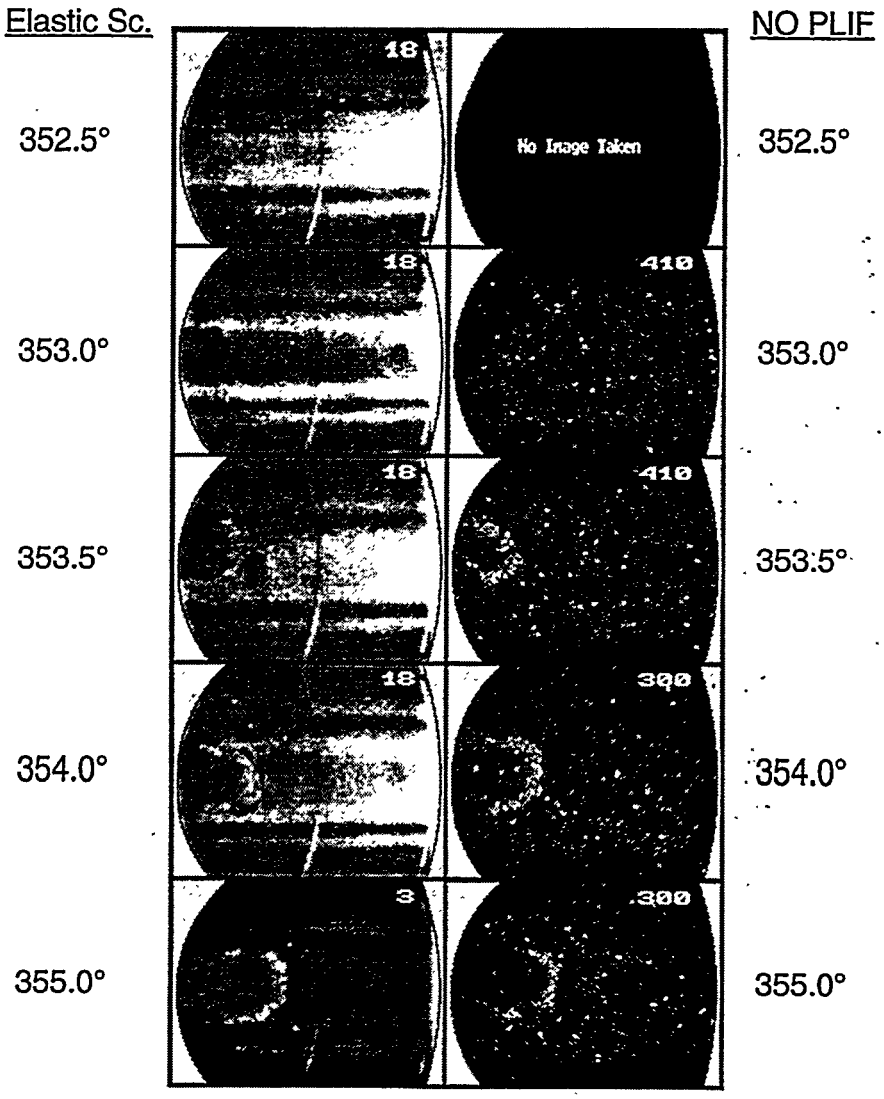

Figure 14. NO PLIF (right) and elastic-scatter (left) images in the plane 10 mm below the cylinder head. The crank angle after TDC exhaust is given at the side of each image, and the field of view is 43 by 33 mm. The number at the upper right of each image is a relative camera gain.

underway and the gases within the fuel jet are less dense than the surrounding air. During this initial portion of the premixed burn there is no signal in the corresponding NO images at the right. Then, at 353.5°, the elastic scatter image shows a signal in the central region of the jet indicating the presence of soot particles, with a very black (low-density) region around the jet periphery where the diffusion flame has just formed. This image corresponds to the 6.5° ASI schematic in Fig. 11. At this crank angle, the NO image now shows a signal in a horseshoe-shaped region around the jet periphery. This same general NO distribution remains through the rest of the sequence presented.

These NO image data strongly support the conceptual model of diesel combustion presented above. As discussed in the description of the model above, the initial premixed portion of diesel combustion is fuel rich (equivalence ratio of 2 - 4). This results in combustion temperatures that are too low to produce NO by the thermal mechanism. Also, oxygen levels are so low that even the "prompt" mechanism does not produce NO at these equivalence ratios [9]. In agreement, the images in Fig. 14 show no NO signal from the premixed combustion area. The conceptual model indicates that the only location for significant NO production up through the end of fuel injection is at the jet periphery on the

lean side of the diffusion flame as shown in Fig. 13. It is at this location, where temperatures are high and oxygen is available, that the images in Fig. 14 show a signal from NO beginning with the onset of diffusion combustion.

CONCLUDING REMARKS

The results presented in this article show that laser-sheet imaging diagnostics have added considerably to our knowledge of DI diesel combustion and emissions-formation. By combining the data from multiple diagnostics a fairly complete picture or "conceptual model" of diesel combustion has been developed. This model covers the diesel combustion process from the start of injection through the first part of the mixing-controlled burn (*i.e.* until the end of injection). It correlates all of the data of the author and coworkers and virtually all the other data in the literature. However, additional work is needed to extend this conceptual model to the late stages of diesel combustion and to determine the effects of walls, swirl, and changes in operating conditions on the reacting diesel fuel jet.

The recent NO imaging results are in full agreement with the conceptual model as presented, and they extend the model by verifying some of the features that were previously hypothesized.

ACKNOWLEDGMENTS

The author would like to acknowledge the contributions of Christoph Espey who has been a co-author on many of the supporting papers referenced here. I am also grateful to Eldon Porter for maintaining the experimental apparatus and for help with the data acquisition. The author would also like to express his gratitude to Patrick Flynn and Roy Primus of the Cummins Engine Co. for their continual strong support of this project.

This work was performed at the Combustion Research Facility, Sandia National Laboratories, Livermore, CA. Support was provided by the U.S. Department of Energy, Defense Programs Technology Transfer Initiative through a cooperative research and development agreement (CRADA) with the Cummins Engine Co. and by the DOE Office of Transportation Technologies through a CRADA with Cummins Engine Co., Caterpillar, and Detroit Diesel Corp.

REFERENCES

1. Dec, J. E., " A Conceptual Model of DI Diesel Combustion Based on Laser-Sheet Imaging," SAE paper no. 970873, 1997.

2. Espey, C. and Dec, J. E., "Diesel Engine Combustion Studies in a Newly Designed Optical-Access Engine Using High-Speed Visualization and 2-D Laser Imaging," *SAE Transactions*, Vol. 102, Sec. 4, pp. 703-723, paper no. 930971, 1993.

3. Espey, C. and Dec, J. E., "The Effect of TDC Temperature and Density on the Liquid-Phase Fuel Penetration in a D.I. Diesel Engine," *SAE Transactions*, Vol. 104, Sec. 4, pp. 1400-1414, paper no. 952456, 1995.

4. Espey, C., Dec, J. E., Litzinger, T. A. and Santavicca, D. A., "Planar Laser Rayleigh Scattering for Quantitative Vapor-Fuel Imaging in a Diesel Jet," *Combustion and Flame*, Vol. 109, 65-86, 1997.

5. Dec, J. E. and Espey, C., "Ignition and Early Soot Formation in a D.I. Diesel Engine Using Multiple 2-D Imaging Diagnostics," *SAE Transactions*, Vol. 104, Sec. 3, pp. 853-875, paper no. 950456, 1995.

6. Dec, J. E. and Coy, E. B., "OH Radical Imaging in a DI Diesel Engine and the Structure of the Early Diffusion Flame," SAE paper no. 960831, 1996.

7. Dec, J. E., "Soot Distribution in a D.I. Diesel Engine Using 2-D Imaging of Laser-Induced Incandescence, Elastic Scattering, and Flame Luminosity," *SAE Transactions*, Vol. 101, Sec. 4, pp. 101-112, paper no. 920115, 1992.

8. Naber, J. D. and Siebers, D. L., "Effects of Gas Density and Vaporization on Penetration and Dispersion of Diesel Sprays," SAE paper 960034, 1996.

9. Miller, J. A. and Bowman, C. T., "Mechanism and Modeling of Nitrogen Chemistry in Combustion," *Prog. Energy Combust. Sci.*, Vol. 15, pp. 287-338, 1989.